Plan for Lectures #4, 5, & 6

Theme Of Lectures: Nano-Fabrication

Quantum Wells, SLs, Epitaxial Quantum Dots

Carbon Nanotubes, Semiconductor Nanowires

Self-assembly and Self-organization

Two Approaches To Nano-Fabrication

Top-down ⇔ Bottom-up

lithography does the work (Top-down)

let the atoms do the work (Bottom-up)

Emphasis Of These Lectures: Atomic Control in the Growth of Nanostructures

Classification of Nanostructures by Dimensionality

2D Quantum wells, superlattices, L-B, membranes, ...

1D Nanotubes, nanowires, nanorods, nanobelts, ...

0D Nano dots from the gas phase (plasma)

Strained epitaxial nano dots

Colloids and nanoparticles by other methods

3D Nanocomposites, filamentary composites, cellular materials, porous materials, hybrids, nanocrystal arrays, block co-polymers,

ZnO Nanowires on Al_2O_3

catalyst-free

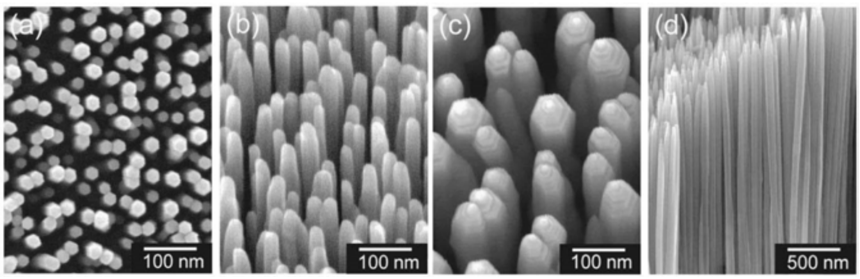

Park et al, APL 02 MOVPE DEZn, O_2, Ar

Initial LT Growth (coarsening) before 400-500^{o}C growth.

Quantum Wells & Superlattices

Si/Ge layers grown by MBE on relaxed SiGe(100)

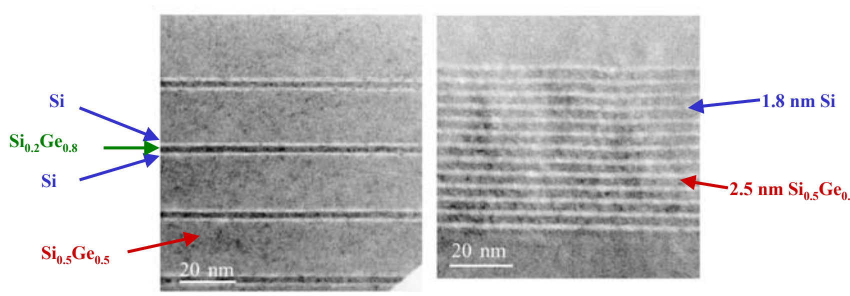

High Resolution Transmission Electron Microscopy (TEM)

Diehl et al, Physica E 2003

Semiconductor Quantum Dots

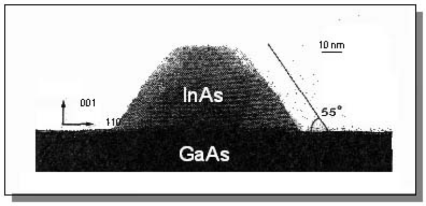

InAs on GaAs
High resolution cross sectional electron micrograph (X-TEM)
Georgsson et. al. Appl. Phys. Lett 1995

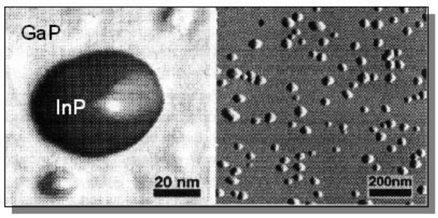

InP on GaP
Atomic Force Microscopy (AFM)
Junno et. al. Appl. Phys. Lett. 1998

Fabrication of Semiconductor Nanostructures

2D **Quantum wells, superlattices, L-B, membranes, ...**

1D **Nanotubes, nanowires, nanorods, nanobelts, ...**

0D **Nano dots from the gas phase (plasma)**

Strained epitaxial nano dots

Colloids and nanoparticles by other methods

3D **Nanocomposites, filamentary composites, cellular materials, porous materials, hybrids, nanocrystal arrays, block co-polymers,**

today's lecture

next 2 weeks

Epitaxial Growth

Pre-Growth Considerations

What substrate to use? (doping, surface orientation, wafer size, pre-pattern, surface cleaning, pre-treatment, etc.)

How to prepare the surface? (in situ cleaning, buffer, surface composition, reconstruction, step management, characterization, etc.)

What structure to grow? (composition, # layers, thickness, doping, morphology, defect level, etc.)

How to grow? (equipment, growth technique, source material, growth rate, temperature, growth monitor, pressure, flow rates, etc.)

Additional processing? (post-annealing, passivation, metallization, cap, etc.)
Ex-situ processing, characterization of device and material quality.

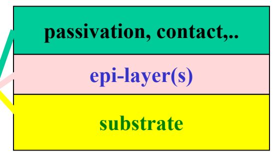

Special Considerations For Nanostructures

Surface Morphology

Strain

Steps, kinks, islands, adatoms.

Surface Energy

Impurity stabilization

Surface Structure & Diffusion Anisotropy

Defects and Inhomogeneity

Molecular Beam Epitaxy (MBE)

Al Cho and John Arthur are given the credit for inventing the molecular beam epitaxy (MBE) technique.

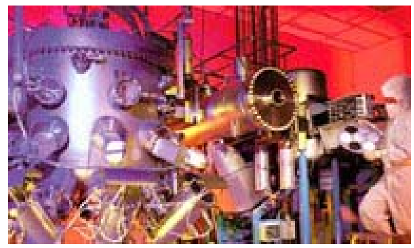

An MBE system is essentially a very clean (UHV) deposition chamber with atomic level control, using (mostly) physical processes.

Differentiations: Solid-source MBE, gas-source MBE, MOMBE, CBE, ...

Metal-organic Chemical Vapor Deposition (MOCVD)

Structure, Lattice Parameter, and Bandgap

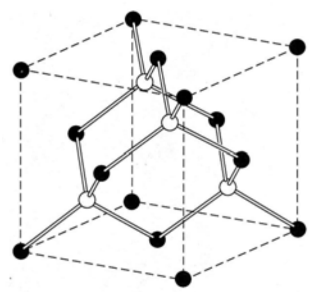

zincblend

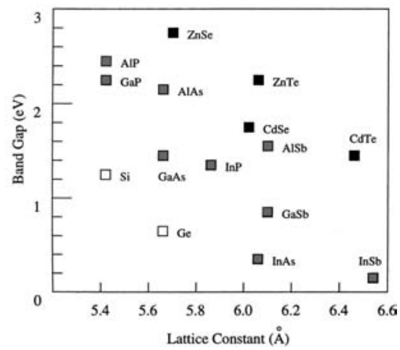

Alloying often allows wide ranges of lattice constants and band gaps.

Common Substrates For Epitaxial Growth

Si(100): **Substrate of choice for Si ULSI device.**

GaAs(100): **Convenient substrate for compound semiconductor devices (heterojunctions, optoelectronic devices, etc.)**

Si(111): **Popular substrate for epitaxial growth of assorted material. Has 7x7 reconstruction, rich in surface science studies. Cleavage surface.**

Sapphire(0001): **Insulating substrate for epi-growth.**

Surface Preparation

Ex situ cleaning and etching

Thermal evaporation of oxide

Sputtering and annealing

Cleaving

H-termination

Buffer growth (MBE,…)

Surface Cleanliness

Auger Electron Spectroscopy (AES)

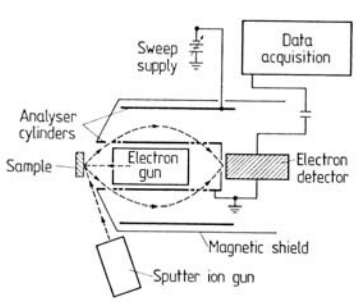

Fig. III.3. Schematic plot of a standard experimental set-up for Auger Electron Spectroscopy (AES). The primary electron beam is generated by an electron gun which is integrated on the central axis of a Cylindrical Mirror Analyser (CMA). An additional sputter ion gun provides the possibility of depth analysis

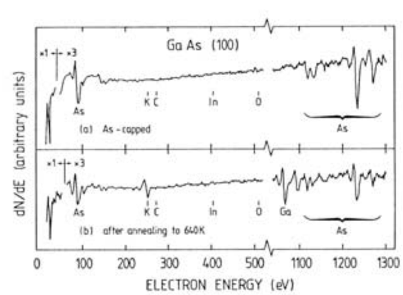

Fig. III.5a,b. Differentiated Auger electron spectra dN(E)/dE measured with a primary electron energy of 2000 eV on a GaAs(100) surface prepared by Metal-Organic Molecular Beam Epitaxy (MOMBE). (a) After the epitaxy process the surface was covered in the MOMBE system by an amorphous arsenic film and transferred through air into the analysis chamber for the AES analysis. This spectrum corresponds to the As-capped surface. (b) After mild annealing to about 300°C the arsenic film is desorbed and the characteristic spectrum of the GaAs surface appears, with very slight contamination due to K [III.4]

Surface Cleanliness

Low Energy Electron Diffraction (LEED)

~55eV
A- & B- $NiSi_2$ on Si(111)

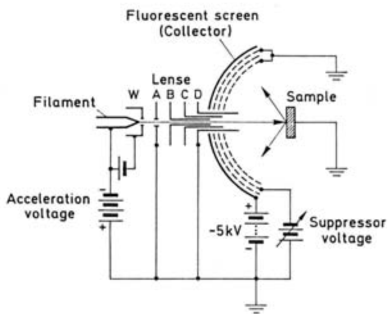

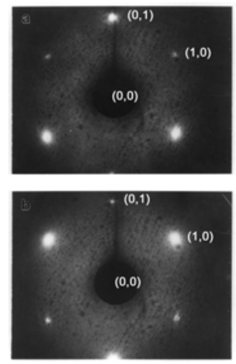

Schematic of a three-grid LEED optics for electron diffraction experiments. The integrated electron gun consists of a heated filament, a Wehnelt cylinder (*W*) and the electron optics containing the apertures A–D. B and C are usually held at potentials between those of *A* and *D*.

Beam energy: ~ 20-200eV

Reconstruction of Si(100) Surface

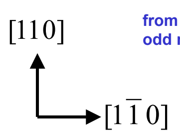

from regions differing by odd number of planes

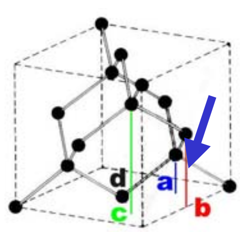

Stacking sequence: -abcdabcd-

Alternating dangling bond direction.

dimer rows

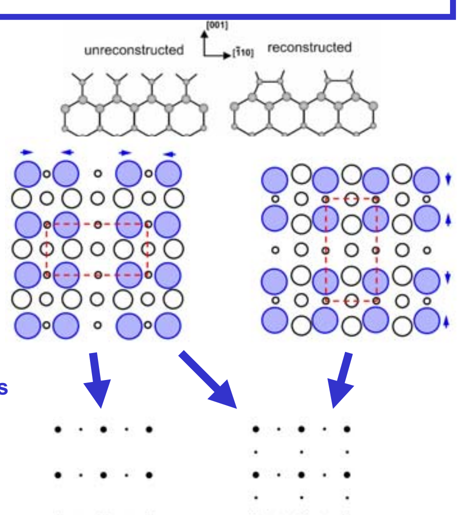

"2x1" **"1x2" plus "2x1"**

Scanning Tunneling Microscopy (STM)

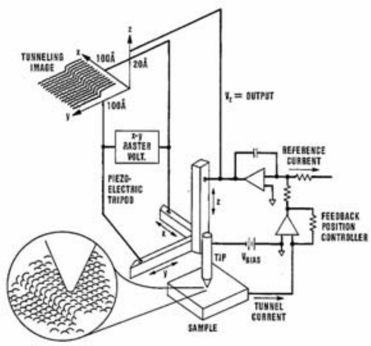

Fig. 6. Schematic diagram of a tunneling microscope. A tungsten tip is mounted on a piezoelectric tripod actuator which can move the tip in the (*x–y*) plane of the sample surface, and in the *z* direction normal to the surface, with atomic resolution. The *x* and *y* piezoactuators that move the tip in the plane of the sample surface are driven by an *x–y* raster scan generator. The actuator that moves the tip in the *z* direction, normal to the sample surface, is driven by a feedback position controller that attempts to maintain the tunnel current at a set reference level by adjusting the tunnel gap width. By plotting the feedback voltage V_z as a function of the tip's *x–y* position on the surface, a tunneling image of the surface is obtained [48].

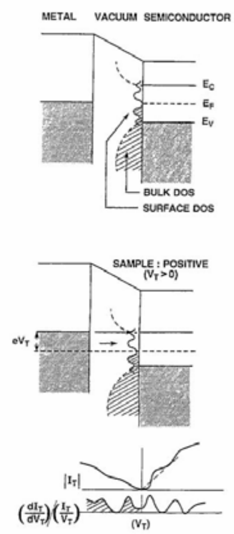

Si(100) Dimer Rows

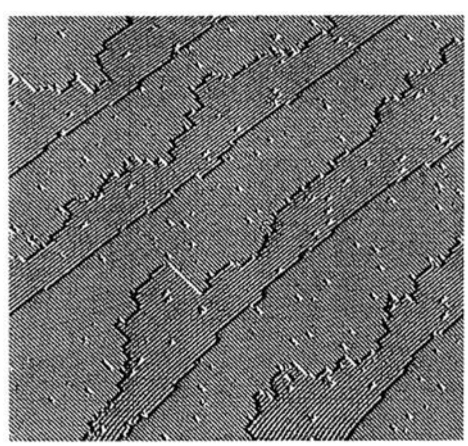

Swartzentruber et al, PRB 1993

Vicinal Si(100) Surface

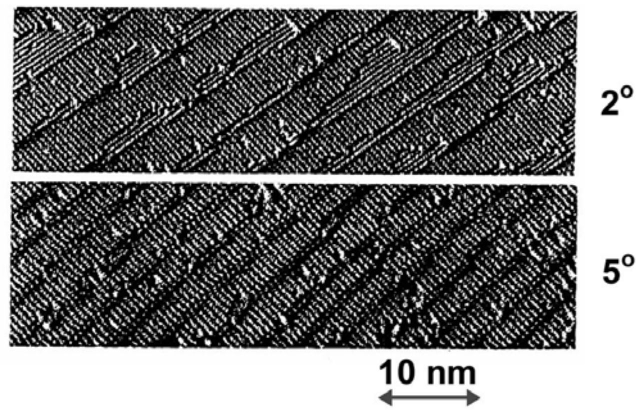

Swartzentruber PRB 1993

Terraces and Steps on Si(100)

Type of Steps:
S_A, S_B, D_A, D_B

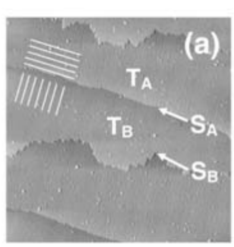

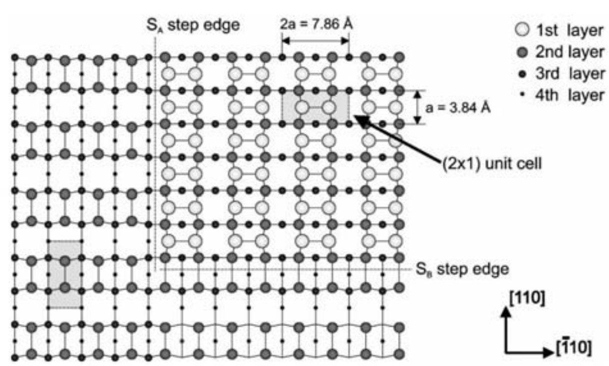

Step A: upper terrace dimer rows are parallel to step
Step B: upper terrace dimer rows are perpendicular to step

Note: dimer direction is perpendicular to dimer row direction!

Calculations (Chadi):
S_A more stable than S_B.
D_B more stable than D_A.
D_B more stable than $S_A + S_B$.

Effect of Strain on the Stability of Si(100) Domains

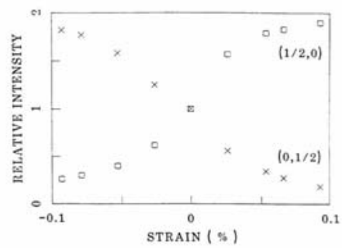

FIG. 1. The ratio of the intensity of the ($\frac{1}{2}$,0) and (0,$\frac{1}{2}$ LEED beams to their values at zero strain plotted as function of the calculated surface strain. The data were measured at fixed position along the bar for various deflections of the enc The domain compressed along the dimer bond is favored.

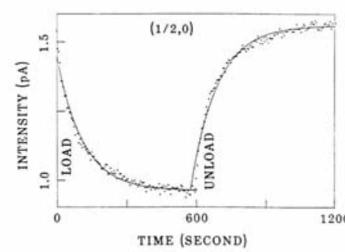

FIG. 3. The intensity of the ($\frac{1}{2}$,0) superlattice reflection as a function of time after applying and removing the external compressive stress. These data were taken at 550°C. The time constant is 114 ± 7 sec.

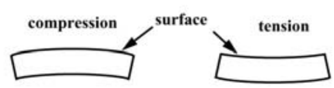

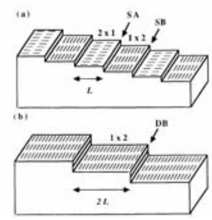

Men et al, PRL 1988

7x7 Reconstruction on Si(111)

unoccup. **occupied**

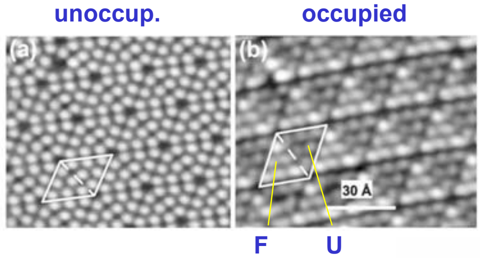

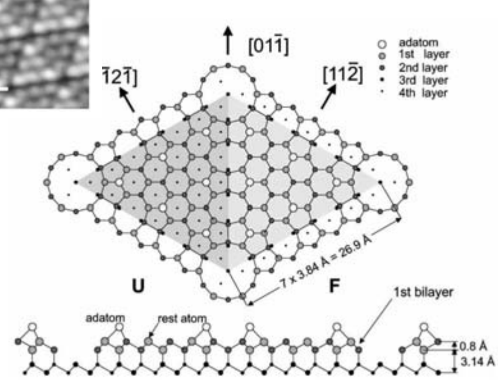

9 dimers
12 adatoms
19 dangling bonds
102 atoms first 3 layers

DAS model of Takayanagi

Reconstruction and Strain

Si(111) above ~850°C	1x1
Si(111) crystal surface	7x7
Si grown on SiGe (tensile)	5x5
Ge(111) crystal surface	C(2x8)
Ge thin layer on Si (compression)	7x7
SiGe grown on Si (mild compression)	5x5

(2m+1)x(2m+1) reconstruction:

3m dimers, m(m+1) adatoms

Reconstructions on (111) relieve compressive stress. Most favorable reconstruction depends on strain condition of semiconductor (layer).

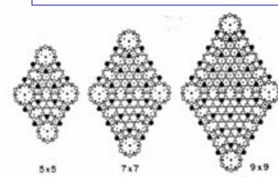

Fig. 65. Top view of the $(2m+1)\times(2m+1)$ DAS family of reconstructions for $m=2,3$, and 4. Shaded large circles are adatoms. Open circles are atoms in the partially faulted double layers directly below. Filled small circles are the bulk unreconstructed double layer of the bulk [37].

Polar and Non-polar Surfaces (Comp. Semicond.)

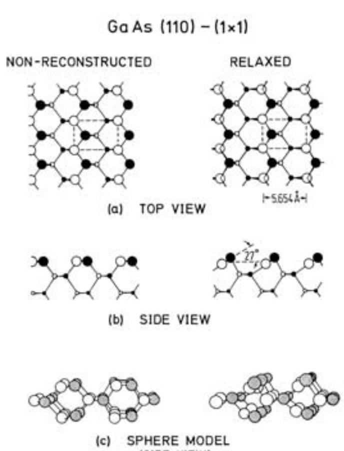

Fig.3.5a-c. Atomic positions of the GaAs(110) surface; ideal, non-reconstructed and relaxed as it appears after cleavage in UHV. (a) Top view; the (1×1) unit mesh is plotted as a broken line. (b) Side view. (c) Sphere model. (*Open circles* designate Ga atoms and *shaded circles* As. *Smaller circles* indicate deeper atomic layers)

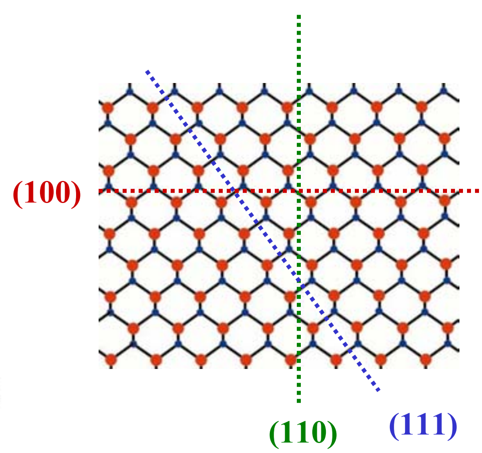

Stoichiometry and Reconstruction on GaAs(100)

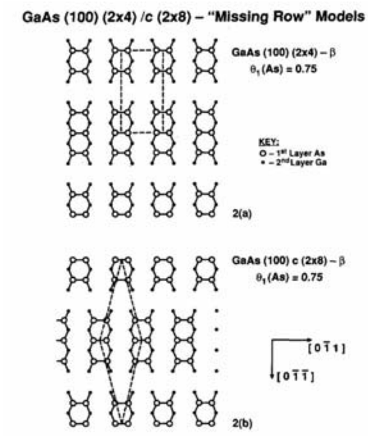

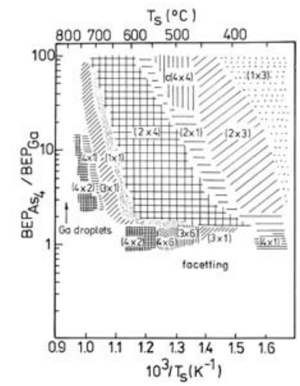

Fig. 1. Surface phase diagram of GaAs(001) for MBE growth on (001) 2° misoriented toward (1$\bar{1}$1) As, growth rate 0.7 ML s^{-1} for $T_s < 630$ °C. The surface reconstructions are plotted versus both substrate temperature T_s and the As_4:Ga flux ratio expressed by the beam equivalent pressure (BEP) ratio.

Farrell & Palmstrom JVST 1990

"2-by" due to As dimers
"by-2" due to Ga-dimers

Misorientation, Steps, Step Bunching, etc.

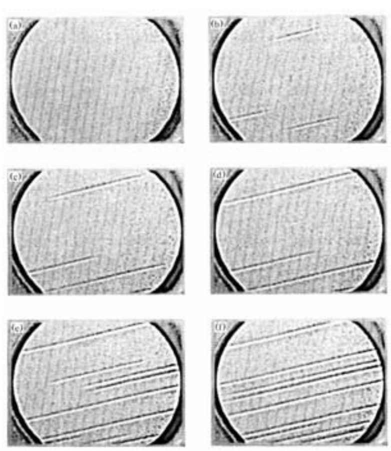

Si(111) 4° toward $[11\bar{2}]$

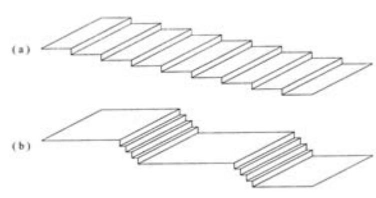

FIG. 1. LEEM images of a vicinal Si(111) surface misoriented by 4° towards the [$\bar{2}$11] direction, as it is quenched through the (7×7)-to-(1×1) transition. The bright regions are (7×7) reconstructed facets. The temperature of (a) is 851 °C; the temperature of (b)–(f) is 848 °C. (a)–(d) are separated by 7.5 s each; (d)–(f) are separated by 37.5 s. The horizontal dimension is ≈ 4 μm.

Phaneuf, et al PRL 1991

$T_o = 857^oC$

Low Energy Electron Microscopy

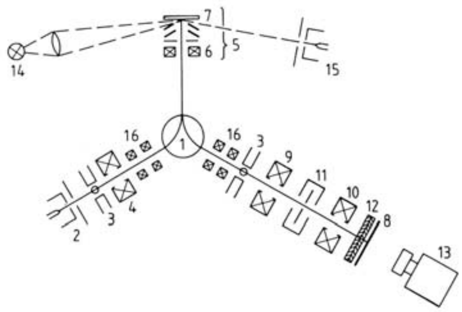

Fig. 1. Schematic of the UHV surface microscope: (1) magnetic deflection field, (2) field emission electron gun, (3) quadrupoles, (4) beam forming lens, (5) cathode lens, (6) stigmator, (7) specimen, (8) screen, (9) intermediate lens, (10) projector lens, (11) filter lens (12) multichannel plates, (13) TV camera, (16) beam alignment coils. For operation as an emission microscope a Hg lamp (14) and a conventional electron gun (15) are attached.

Ernst Bauer

LEEM Images of Si(100)

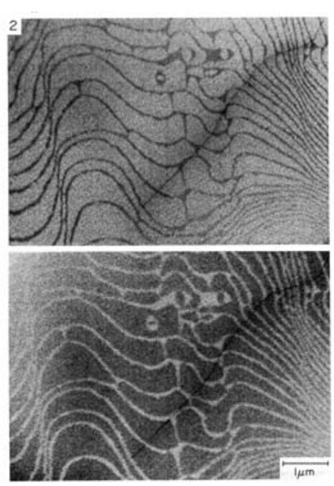

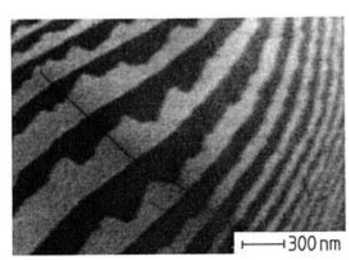

Tilt sample slightly
toward [110] or [-1 10]

Wulff Plot and Step Bunching

Surface energy

equilibrium crystal shape

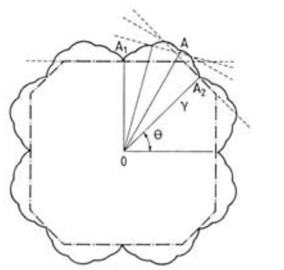

Schematic plot of the scalar surface tension γ(hkl) in polar coordinates as a function of angle Θ (describing the normal directions to the (hkl) planes). This Wulff construction [3.3, 4] yields the equilibrium shape of a solid (*dash-dotted*) as the inner envelope of the so-called Wulff planes, i.e., the normals to the radius vectors (*broken lines*)

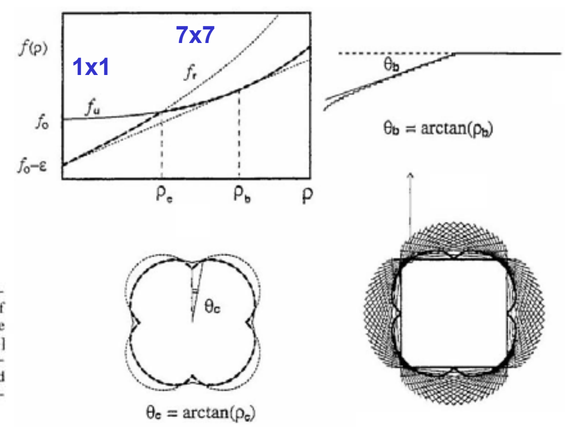

Proof of Wulff Construction

Let (one half of) the surface of a crystal with equilibrium shape be represented by *h(x,y)*, then the surface normal $\hat{n}$ is given by (cap indicates unit vector)

$$\hat{n} = \nabla g / |\nabla g| \qquad (1)$$

where $g(x, y, z) = z - h(x, y)$. Therefore,

$$\hat{n} = \left[-(\frac{\partial h}{\partial x})\hat{x} - (\frac{\partial h}{\partial y})\hat{y} + \hat{z} \right] \left((\frac{\partial h}{\partial x})^2 + (\frac{\partial h}{\partial y})^2 + 1 \right)^{-1/2} . \qquad (2)$$

An element of the surface area, *dA*, is given by

$$dA = \left((\frac{\partial h}{\partial x})^2 + (\frac{\partial h}{\partial y})^2 + 1 \right)^{1/2} dx\, dy \ . \qquad (3)$$

The total surface energy, which must be minimized, is

$$\iint \sigma(\partial h/\partial x, \partial h/\partial y) \cdot \left((\frac{\partial h}{\partial x})^2 + (\frac{\partial h}{\partial y})^2 + 1 \right)^{1/2} dx\, dy \ , \qquad (4)$$

and the constant volume constraint is

$$\iint h \ dx\, dy = \text{constant.} \qquad (5)$$

This is a typical problem which can be solved by Lagrange's undetermined multiplier method. The solution is

$$h = x(\frac{\partial h}{\partial x}) + y(\frac{\partial h}{\partial y}) + \sigma \lambda \left((\frac{\partial h}{\partial x})^2 + (\frac{\partial h}{\partial y})^2 + 1 \right)^{1/2} , \qquad (6)$$

where λ is a constant (multiplier). Since a radius vector to any point on the equilibrium surface is

$$\vec{r} = x\hat{x} + y\hat{y} + h\hat{z} \ , \qquad (7)$$

one can combine Eqs. (2), (6), and (7) to arrive at

$$\vec{r} \cdot \hat{n} = \lambda \sigma \ , \qquad (8)$$

which simply describes the condition that $\vec{r}$ lies on the inner envelope of the Wulff construction.

Si Equilibrium Crystal Shape

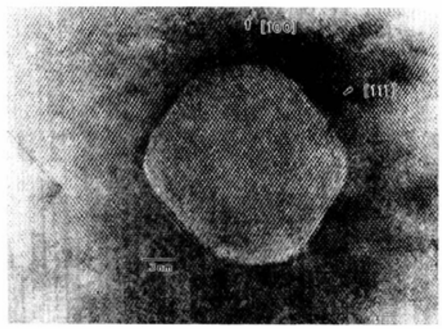

FIG. 1. The equilibrium shape of Si. Typical annealed void shape imaged in high resolution down ⟨110⟩ axis. Void is small enough to be completely enclosed in transmission electron microscopy cross section. Note flat {111} facets and rounded {100} facets, and curved facet intersections at {100} and near {311}.

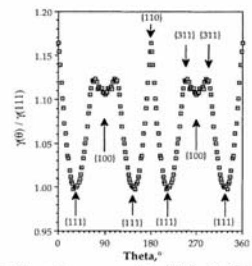

FIG. 2. The surface energy plot $\gamma(\theta)$ for Si. Surface energy ratios extracted by reverse Wulff construction from voids such as that in Fig. 1. Averaged over three particles and symmetrized on the assumption that {110} and {001} are both mirror planes.

Eaglesham et al PRL 1993

Steps and Adatoms: Key to Surface Dynamics

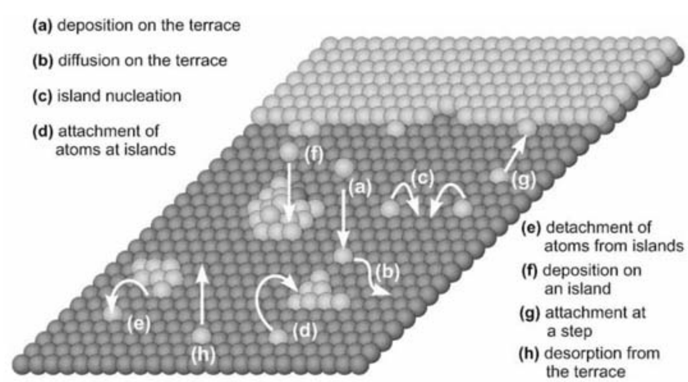

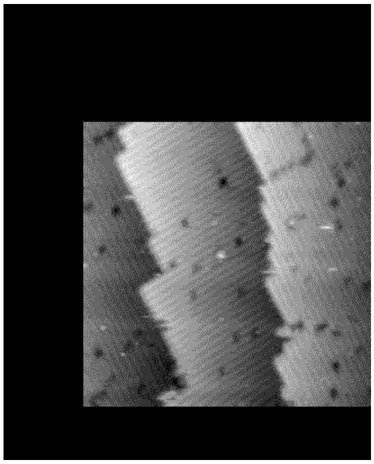

STM image of the Si(001)-(2 × 1) showing the fluctuations of step edges at 693K.
Size= 300 × 300 Å Frame Rate= 1/31sec.

E. Ganz, Univ. Minn.

Adatoms and Step Fluctuation

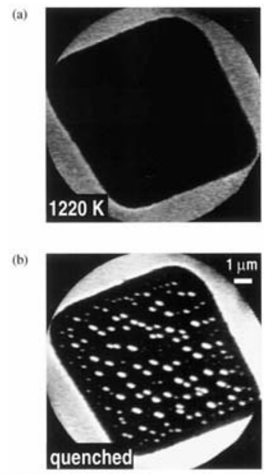

FIG. 1. Dark-field ($\frac{1}{2}$,0) LEEM images of a large atomically flat terrace on Si(001) imaged at 1220 K (a) and after quenching (b).

Tromp et al, PRL 1998

Island Coarsening

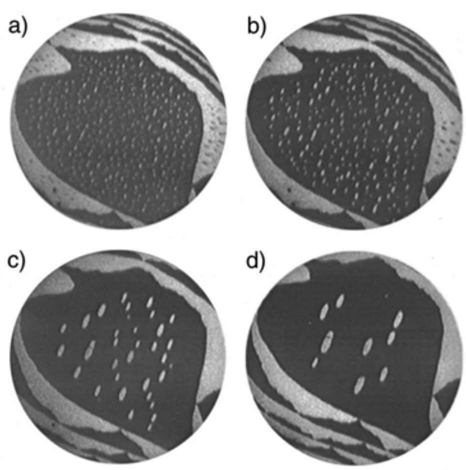

FIG. 1. LEEM images of ripening of single atomic layer height islands on Si(001) at various times after the temperature was increased to 670 °C: (a) 10 s, (b) 50 s, (c) 400 s, and (d) 1300 s. Alternate dark and bright regions differ in height by one atomic layer (0.096 nm). The field of view is 5.5 μm.

Si(100)

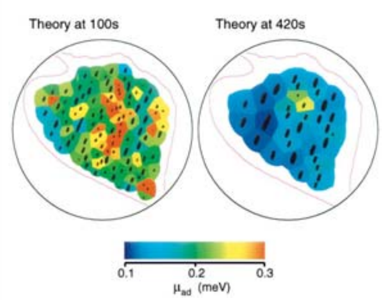

Assume spatial variation of chemical potential for adatoms.

Bartelt et al, PRB 1996

Fluctuation In Island Shape

STM images showing the fluctuations of islands at 620K. The edge rows of islands fluctuate the fastest, and when fluctuations at one's two ends cross, the row disappears. Due to the sticking anisotropy, it is then difficult to nucleate a new row, and the island shrinks. Note that the small lower right hand island disappears all together. Size= 350 × 350 Å Frame Rate= 1/32min.

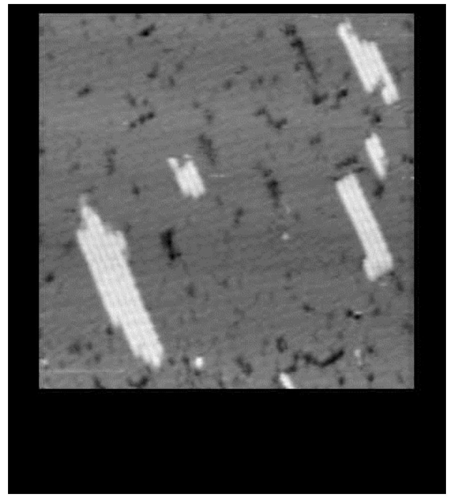

E. Ganz, Univ. Minn.

Equilibrium Island Shape

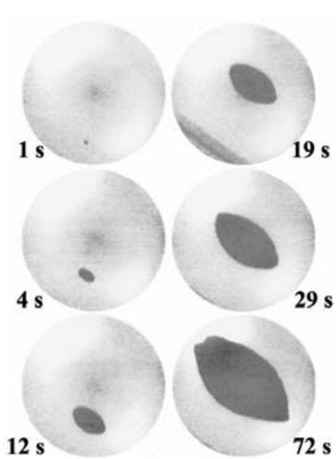

FIG. 1. Evolution of 2D Si island size and shape on an extremely large ($10\times15\ \mu m^2$) single-domain Si(001) terrace during very slow, near-equilibrium, chemical beam epitaxy of Si at 855 °C. The time after observing island nucleation is given in seconds. The island shape evolves with increasing island size, from initially elliptical to "American-football"-like and eventually with 2D faceting (swallow tail at $t=72$ s) for island diameters larger than 6 μm. The field of view is 9 μm. The frame at $t=19$ s shows part of one long mesa edge (gray area at lower left); the base terrace extends beyond the field of view in all other frames. Inhomogeneities in the image (bright area at the corner of the terrace) are due to imperfect focus and inhomogeneities in the channel plate.

field of view: 9μm

Zielasek, et al PRB (2001).

Coarsening On Si(111)

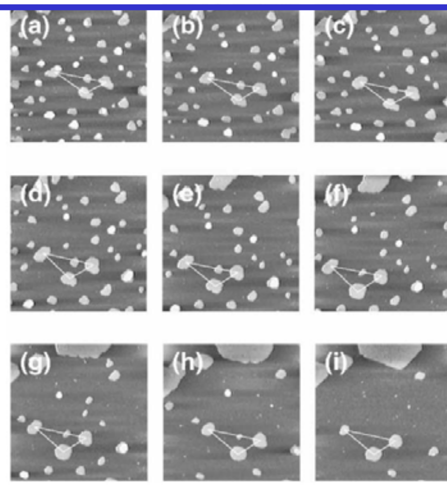

Coarsening

Oswald Ripening

Fig. 10. Coarsening of Si islands on Si(1 1 1) (3000 Å × 3000 Å). The temperature is increased from 725 to 825 K from (a) to (i), respectively. During Ostwald ripening decay of smaller islands and growth of larger islands at domain boundaries is observed.

Voigtlander, SSR 2001

Adatoms

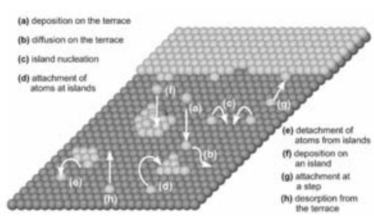

There is a finite density of “adatoms” on the terraces of a surface. The higher the temperature, the higher the adatom concentration. Some adatoms are not visible in STM.

Adatoms are continuously captured and released by the steps. Adatoms have a finite desorption rate, which increases with temperature.

Adatoms can be captured by “defects”, and they can group together to form islands.

Si(100): Dimer Diffusion Along Row

STM images showing the diffusion of a single dimer along a dimer row at 410K. This is composed of *empty state* images, so the surface rows appear *dark* and the troughs appear *bright*. The dimer's orientation flips between parallel and perpendicular to the rows (types A and B respectively) while it progresses along the row; however, at this temperature the two orientations are indistinguishable. Size= 166 × 166 Å Frame Rate= 1/18sec.

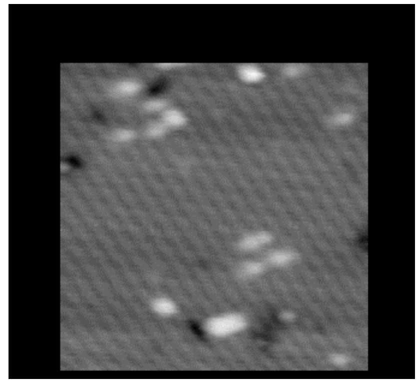

E. Ganz Univ. Minn.

Ehrlich-Schwoebel Barrier

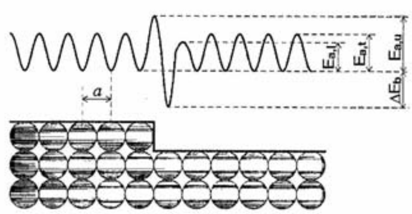

Fig. 16. Simple models of atomistic diffusion are based on the idea of discrete hops between preferred binding sites as shown here. (However, diffusion by an exchange mechanism in which one atom displaces a neighbor is also known to be a lower-energy path in many cases.) On the terraces, the bindings sites might be on-top, bridge or hollow sites. In this illustration, the binding sites are assumed to have the same spatial periodicity as the substrate atoms (which would not be the case for instance for bridge bonding), and a simple activation barrier $E_{a,t}$ for hopping between sites. In moving onto a step binding site (which may have many possible binding configurations), from the upper step–edge, it is physically reasonable to assume that the activation state involves a lower-coordination than for hopping on the terrace, and thus will have a higher activation energy, $E_{a,u}$. It might also be assumed that hopping onto the step from the lower terrace would involve a somewhat more accessible activated state, and thus a slightly lower activation energy $E_{a,l}$. Calculated values of activation energies near steps are listed in Table 6.

Ehrlich and Schwoebel (independently) proposed that it was more difficult for adatoms to hop down a step.

Deposition (=Adding Adatoms)

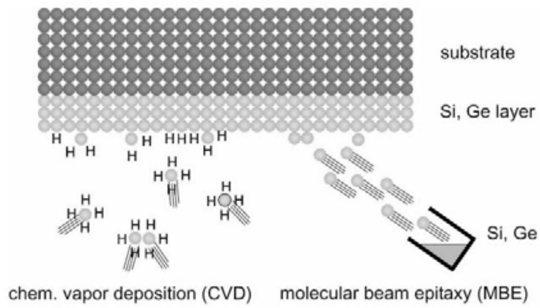

Deposition increases the density of adatoms (dramatically).

$$\text{Supersaturation} = \frac{\text{deposition rate}}{\text{desorption rate}}$$

At a Si deposition rate of 0.4nm/s, the supersaturation varies from 4.4E3 at 950°C to 3E16 at 450°C.

Understanding Growth At The Atomic Level

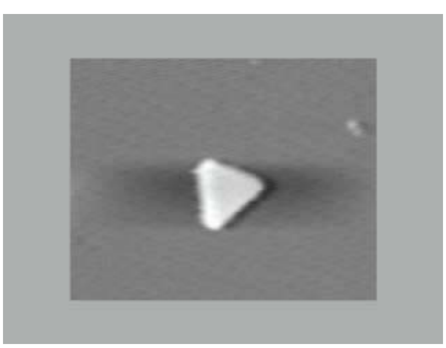

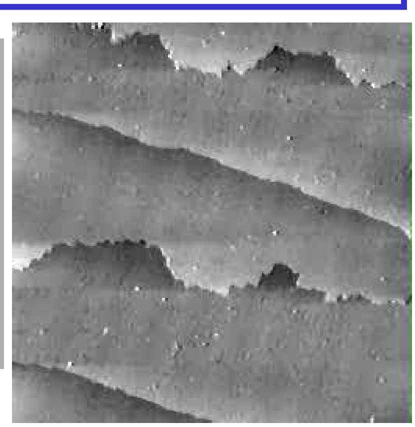

We need control on the atomic level, in order to grow nanostructures.

Voigtlaender et al, PRL 1998.

Pre-existing Steps And Adatoms

$$x_s^2 \frac{\partial^2 \varphi}{\partial y^2} - \varphi + \tau_s v \frac{\partial \varphi}{\partial y} = 0$$

BCF Theory (Burton, Cabrera, and Frank)

low supersaturation - step flow

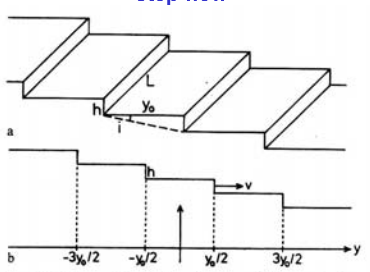

Fig. 1. (a) Scheme of a misoriented surface with low-index planes separated by misorientation steps. (b) Moving coordinate system used in Sect. 1

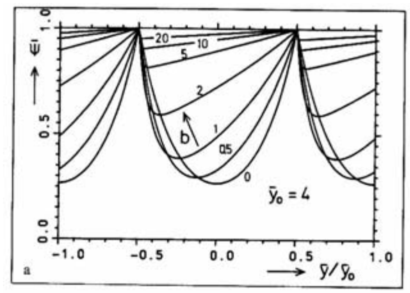

Fig. 4a and b. Supersaturation difference $\bar{\varphi}$ as a function of $\bar{y}/\bar{y}_0 = y/y_0$ for $\bar{y}_0 = 4$ (a) and $\bar{y}_0 = 20$ (b) and for various b values

Homoepitaxial Growth On Si(111)

Tung PRL 1989

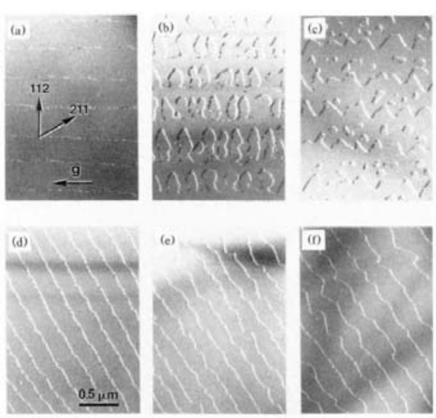

FIG. 3. Plan-view TEM micrographs illustrating the initial stages of Si homoepitaxial growth at 650 °C. (a) A substrate with a small misorientation toward [11$\bar{2}$]. (b),(c) Surfaces after the deposition of 1- and 2-ML Si, respectively, on this substrate. (d) A substrate with a small [2$\bar{1}\bar{1}$] misorientation; (e),(f) the topographies after the deposition of 1- and 2-ML Si, respectively.

2 -1 -1 steps preferred over 1 1 -2 steps

Step Flow vs. Nucleation on Terraces

Tung PRL 1989

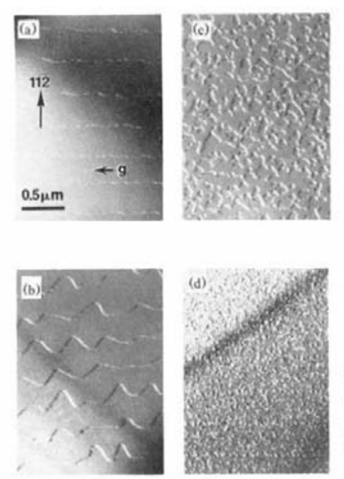

FIG. 2. Dark-field TEM images of $CoSi_2$ layers grown on Si surfaces after Si MBE growth. (a) Substrate surface, and (b)–(f) surfaces after the growth of 50-Å Si at a rate of 0.5 Å/s. Deposition temperature was (b) 750 °C, (c) 650 °C, and (d) 550 °C. (a)–(d) were imaged with $\mathbf{g}=[\bar{2}20]$.

Reflection High Energy Electron Diffraction (RHEED)

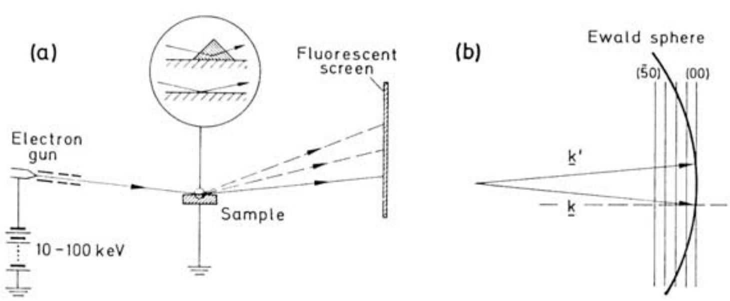

Fig. VIII.4. (a) Schematic of the experimental set-up for RHEED. The inset shows two different scattering situations on a highly enlarged surface area: surface scattering on a flat surface (below) and bulk scattering by a three-dimensional crystalline island on top of the surface (above). (b) The Ewald sphere construction for RHEED. **k** and **k'** are primary and scattered wavevectors, respectively. The sphere radius k = k' is much larger than the distance between the reciprocal lattice rods (hk). For more details, see Sect. 4.2 and Figs. 4.2,3

RHEED From GaAs(100)

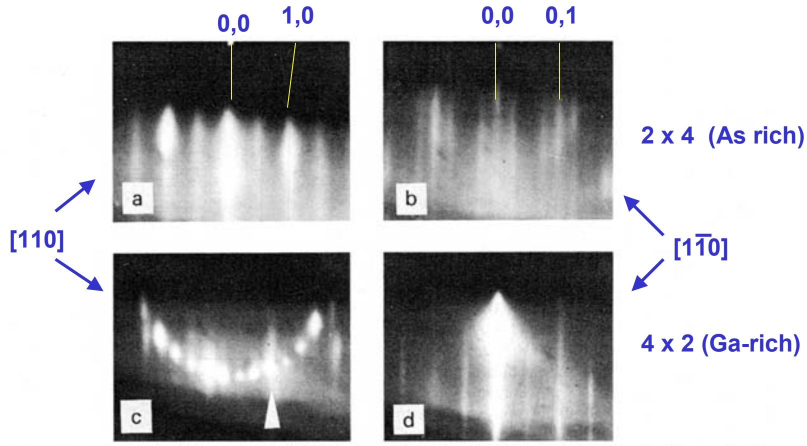

Fig. 3. RHEED patterns recorded during growth in the [110] (a, c) and [$\bar{1}$10] azimuth (b, d) at growth conditions leading to a (2 × 4) (a, b) and a (4 × 2) reconstruction (c, d), respectively. Growth parameters: (a, b) $T_s = 625\,°C$, $BEP_{As_4} : BEP_{Ga} = 40$, (c,d) $T_s = 704\,°C$, $BEP_{As_4} : BEP_{Ga} = 3$.

Nucleation of Steps (high supersaturation) RHEED Oscillation

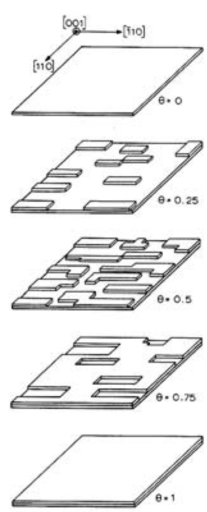

θ is fractional layer coverage

Fig. 6. Real space representation of the formation of a single complete layer

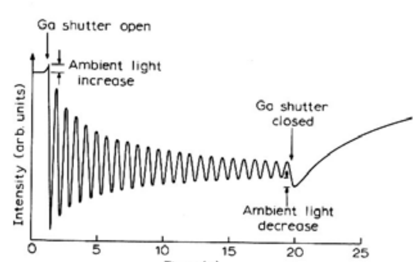

Fig. 1. Intensity oscillations of the specular beam in the RHEED pattern from a GaAs (001)−2×4 reconstructed surface, [110] azimuth. The period exactly corresponds to the growth rate of a single Ga+As layer and the amplitude gradually decreases. Note that the marked inflections at the beginning and end of growth result from ambient light change as the shutters are opened and closed

RHEED Oscillations During Si MBE

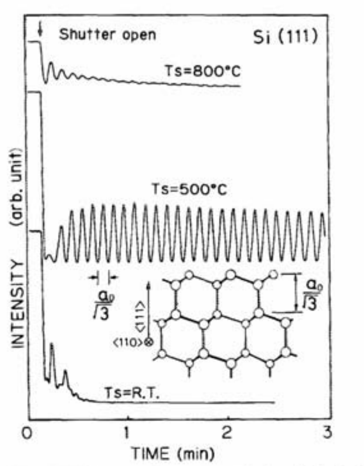

FIG. 4. RHEED intensity oscillation on Si(111) taken from ⟨110⟩ azimuth, T_s = R.T., 500 °C, and 800 °C.

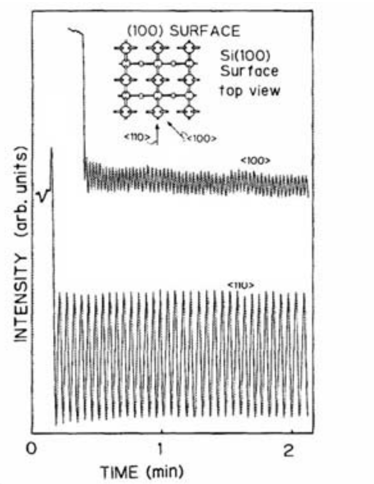

FIG. 3. RHEED intensity oscillation on Si(100) taken from various azimuths, T_s = 400 °C.

Preferential Nucleation Of Islands

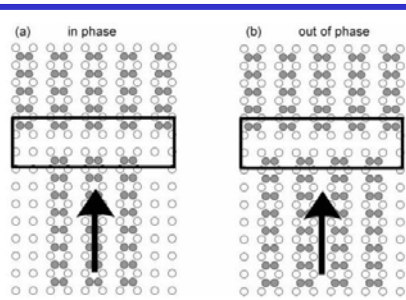

"Anti-Phase Domain Boundary"

Si(100)

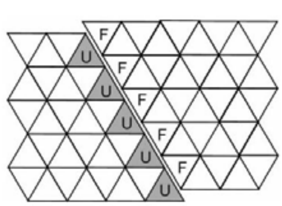

Si(111)

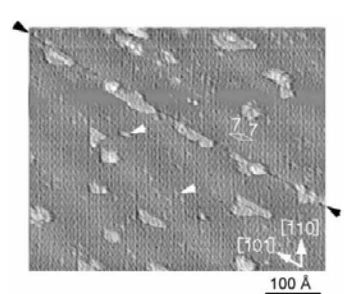

Si Growth On Si(100) Terraces

STM images showing the growth of islands at 533K. Coverage increases from 0 to 0.1 ML at a rate of approximately 0.01 monolayers deposited per frame. The movie begins with the clean substrate before deposition. At this temperature 1-D islands form and coalesce. Size= 800 × 800 Å Frame Rate= 1/33min.

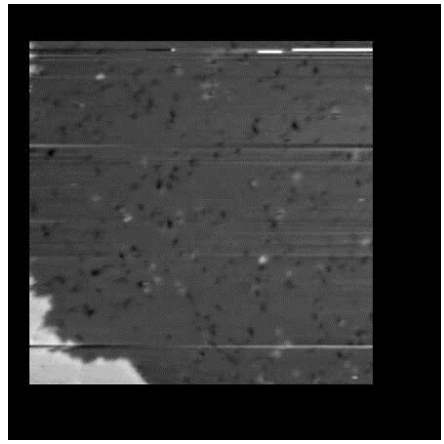

Property of E. Ganz Phys. Dept. Univ. Minn.

Roughening Of Surface Morphology

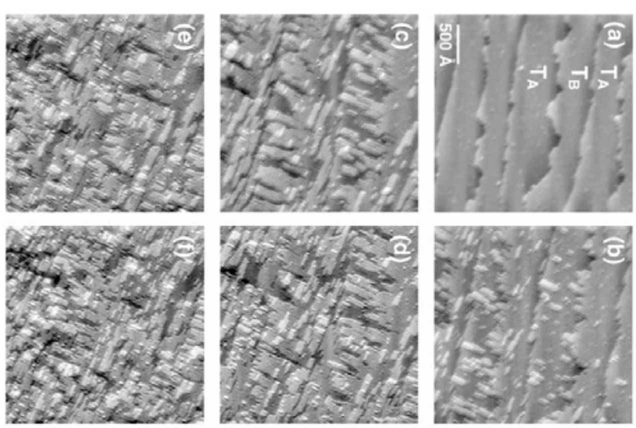

Island nucleation growth mode of Si on Si(0 0 1) ($T = 575$ K, $F = 0.6$ ML/h, 2500 Å × 2500 Å). The straight S_A and the rough S_B steps run horizontally. The terraces, divided by the monoatomic steps, descend from the top to the bottom of the image. In (b), nucleation of elongated islands is observed. During further growth three open layers are observed on each terrace: one layer being closed, one main growing layer, and one layer with islands nucleating on the growing layer. The coverages in images (b)–(f) are 0.34, 0.67, 1.02, 1.34, and 1.67 ML, respectively.

Heteroepitaxial Growth Issues

Lattice mismatch, misfit dislocations, strain inhomogeneity, other strain-related issues

Dissimilar structure, symmetry-related defects, interface energy, nucleation issues, ...

Inter-diffusion, segregation, phase separation, ...

Interface dipole, valence mismatch, ...

Common Lattice Matched Systems

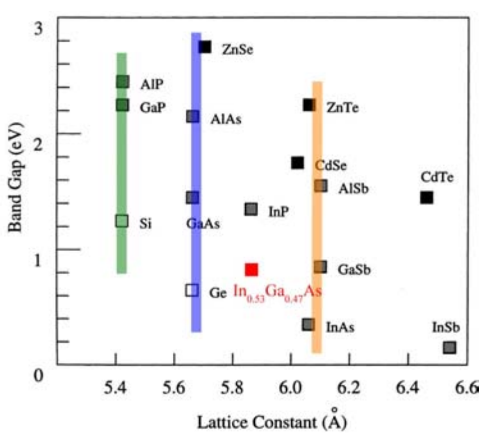

SOME COVALENT III–V COMPOUNDS*

	Al	Ga	In
P	5.45	5.45	5.87
As	5.62	5.65	6.04
Sb	6.13	6.12	6.48

* All have the zincblende structure. The side of the conventional cubic cell (in angstroms) is given.

GaAs ⇔ AlAs

InP ⇔ InGaAs

GaSb ⇔ InAs

GaN ⇔ AlN (wurzite)